Appl. Phys. A 67, 79–87 (1998)

Applied Physics A
Materials
Science & Processing

Electronic structure and quantum transport in carbon nanotubes

J.-C. Charlier, J.-P. Issi

Université Catholique de Louvain, Place Croix du Sud 1, B-1348 Louvain-la-Neuve, Belgium
(E-mail: charlier@pcpm.ucl.ac.be, issi@pcpm.ucl.ac.be)

Received: 3 April 1998

Abstract. The electrical properties of various forms of carbon nanotubes are presented with particular emphasis placed on individual multi-wall and single-wall tubes. After a brief survey of the electronic structure of single-wall carbon nanotubes, electronic transport mechanisms are overviewed in relation with the dimensionality of the carbon system. Typical quantum aspects of low temperature electronic conduction for low dimensionality encountered in some carbon nanotubes are discussed.

PACS: 71.15.Fv, 71.20.Tx, 72.80.Rj, 73.23.-d

It was recently shown [1, 2] how the wealth of information provided by electrical resistivity measurements obtained on carbons and graphites helps improve our understanding of conduction mechanisms in solids. This is particularly true when quantum aspects of conduction are considered. Among the results of measurements available for the large variety of carbon forms, those recently performed on carbon nanotubes have significantly contributed to this situation.

Carbon nanotubes (CN) are fascinating mesoscopic systems on which the various aspects of electronic structure and quantum transport can be tested. To the low dimensionality of these systems is associated specific band structures from which results unusual transport properties, which are further accentuated by their small dimensions with respect to the various electronic characteristic lengths (Sect. 1.2.1). This is in addition to the fact that their parent carbons and graphites exhibit various aspects of conduction which cover a large spectrum of solid state conduction.

Even in the higher temperature range where we can approach the transport properties by means of semiclassical approximations, the behavior is odd as compared to typical 3D metals and semiconductors. Indeed, in addition to the effects of small dimensions and low dimensionality, one has to consider the specific properties of carbons and graphites relative to typical conductors:

– the *semimetallic behavior* due to the presence of a small density of electrons and holes, which has a drastic effect on the band structure and on the scattering mechanisms inherent to small Fermi surfaces [3]
– the possibility of *intercalation*, and to a lesser extent, *doping*, and its effects.

At low and ultralow temperatures, specific effects show up in the propagation and scattering of charge carriers revealing quantum effects at the macroscopic scale. These effects are magnified in the presence of weak disorder. These *quantum aspects of conduction* are revealed by the *weak localization* effects and *Coulomb interaction* and the *universal conductance fluctuations* in the quasi-ballistic regime.

In order to interpret electronic transport results we need to know about the electronic distribution and some characteristic lengths describing the regime of propagation and electron collision events. In CNs this means that we must have a model for the Fermi surface and the order of magnitude of the various characteristic lengths. Besides, the defect structure is an essential ingredient, since its presence is necessary to generate quantum interferences, when applicable.

There is now experimental evidence that multi-wall carbon nanotubes (MWNT) are 2D electrical conductors, while infinitely long single-wall nanotubes (SWNT) exhibit 1D conduction. Oddly enough, for the latter case we are facing an exceptional physical system; a 1D conductor without Peierls' distortion. Whether single- or multi-wall, we will show below that there is a lot of interesting physics in these systems.

The results of measurements on CNs have revealed so far three interesting pieces of information. MWNT behave as an ultimate carbon fiber. At high temperature their electrical conductivity may be described by means of a semiclassical model similar to that applicable to graphene layers in the bulk material. At low temperature they reveal 2D quantum transport features, some of them similar to that previously observed on graphite (weak localization) and some new aspects which can only be observed in its mesoscopic form (universal conductance fluctuations). In addition, SWNTs behave as pure quantum wires, which if limited in length may reduce to a quantum dot. So, each type of nanotube has its own features which are strongly dependent on the dimensionality of the system.

In the following, we shall make a clear distinction when considering conduction in multi-wall (Sect. 2.1) or single-wall (Sect. 2.2) carbon nanotubes. Indeed, it is found that to a given dimensionality is associated specific band structures and quantum transport aspects at low temperature.

1 Theoretical frame

1.1 Electronic structure

Carbon nanotubes have extraordinary electrical properties which derive from the well-known hybridization process of carbon bonds, their unique quasi-one-dimensional nature, and their cylindrical symmetry, that could lead to ideal electrical connectors in future technology [4]. Microscopically, a nanotube consists of one (single-wall [5, 6]) or more (multi-wall [7]) coaxial cylindrical rolled-up graphene sheets, separated by approximately the interlayer distance of graphite (0.34 nm). The size distribution is 0.8–3 nm diameter for single-wall nanotubes and 2–30 nm diameter for multi-wall nanotubes, both being generally microns in length, and also often observed in bundles [8, 9].

With the notion of helicity introduced by Iijima [7], the electronic properties of carbon nanotubes have been studied extensively in many theoretical works [10–15]. All these calculations lead to one important conclusion: the electronic properties of the nanotube should vary in a periodic way from metallic to semiconductor as a function of both the diameter and the helicity. Using Fig. 1a, the chirality and the tube diameter of any graphene tubule can be specified in terms of the chiral vector $\boldsymbol{C}_h = n\boldsymbol{a}_1 + m\boldsymbol{a}_2$ which connects two crystallographically equivalent sites on a 2D graphene sheet [11].

The construction in Fig. 1a shows the chiral angle θ with respect to the zigzag direction ($\theta = 0$) and the unit vectors $\boldsymbol{a}_1$ and $\boldsymbol{a}_2$ of the hexagonal honeycomb lattice. The armchair tube (Fig. 1a) corresponds to $\theta = 30°$ on this construction. An ensemble of possible vectors specified by pairs of integers (n, m) denoting the vector $\boldsymbol{C}_h = n\boldsymbol{a}_1 + m\boldsymbol{a}_2$ is given in Fig. 1b. In the (n, m) notation, the vectors $(n, 0)$ denote zigzag tubes, the vectors (n, n) denote armchair tubes and all the other vectors (n, m) where $n \neq m \neq 0$ correspond to chiral tubes [11].

From a theoretical standpoint, single-wall tubes are interesting as examples of a one-dimensional periodic structure along the tube axis. Confinement in the radial direction results from the monolayer thickness of the tubule. Unless the tube diameter is extremely small, its band structure somewhat resembles that of graphite. The main difference between graphite and the tubule lies in the periodic boundary conditions. A graphite sheet is regarded as an infinitely extended system, and an artificial periodic boundary condition is imposed on a macroscopic scale. This results in the usual Bloch wave functions labeled with wave vectors in the first Brillouin zone. For a tubule, while the boundary conditions along the tube axis are the same as for graphite, the periodic boundary condition is imposed for a finite period along the circumference and allows only a few wave vectors to exist in the circumferential direction. This results in Bloch wave functions with discretely selected wave vectors.

Figure 2 illustrates band structures for zigzag and armchair conformations where the C−C bond is, respectively, parallel and perpendicular to the tube axis. 2D graphite is

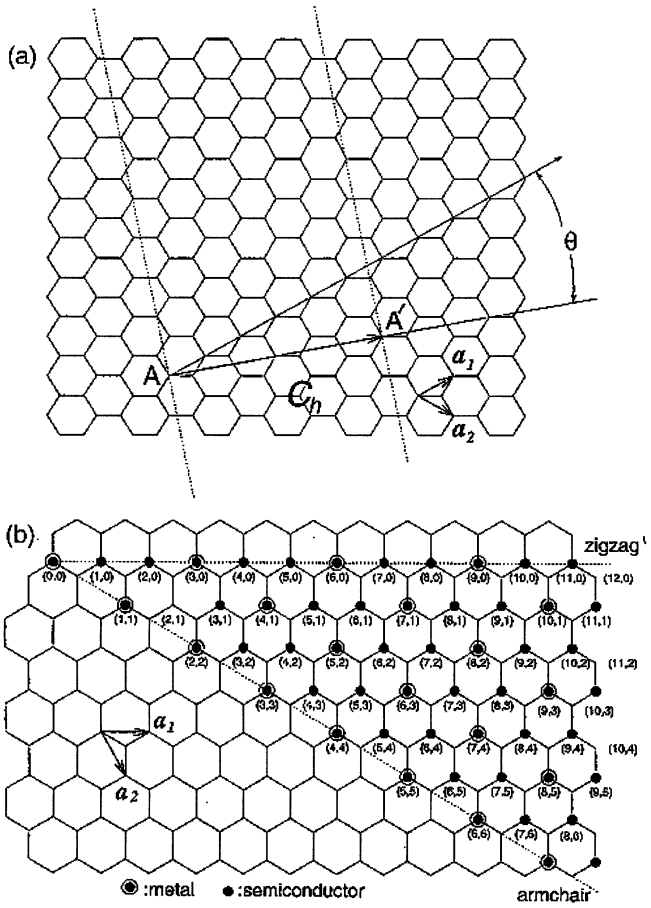

Fig. 1. a The vectors AA' or $\boldsymbol{C}_h = n\boldsymbol{a}_1 + m\boldsymbol{a}_2$ on the honeycomb lattice defined by unit vectors, $\boldsymbol{a}_1$ and $\boldsymbol{a}_2$, and the chiral angle θ with respect to the zigzag axis. **b** A graphite sheet that, when rolled up in such a way as to superimpose the origin (0, 0) on a given hexagon in the sheet, a nanotube will result with the properties indicated in the edge of each hexagon: *large dots* and *small bullets*, denoting metallic (or narrow band gap semiconductor) and moderate band gap semiconducting behavior, respectively [11]

a zero-gap semiconductor with bonding and antibonding π bands, degenerate at the K-point zone corner of the 2D hexagonal Brillouin zone. When a tubule is constructed from a graphite sheet, the periodic boundary condition along the circumference allows wave vectors in certain directions in the Brillouin zone of graphite. For a $(n, 0)$ zigzag tube, the vertical lines are found to cross the points which divide the straight line of doubled $\Gamma - M$ into n parts. Therefore, if a vertical line crosses the K point, namely, if n is a multiple of 3, the tubule might be a metal (Fig. 2a). However, the degenerate point is actually moved from the K point to positions slightly away from the 2D hexagonal Brillouin zone edges, because the electron transfer is enhanced in the circumferential direction due to the curvature of the tube surface. The band structure of the $(12, 0)$ zigzag tube exhibits an energy gap of 8 meV at the Γ point, characterizing a narrow-gap semiconductor, not a metal. Following the derived rule, if n is not a multiple of 3, the zigzag tube possesses a wider band gap. The band structure of the $(11, 0)$ zigzag tubule exhibits an energy gap of 0.8 eV at the Γ point, characterizing a moderate-gap semiconductor (Fig. 2b). In these two band structures, bands higher than the Fermi level (E_F) are antibonding π bands. Bonding π bands are located at energies

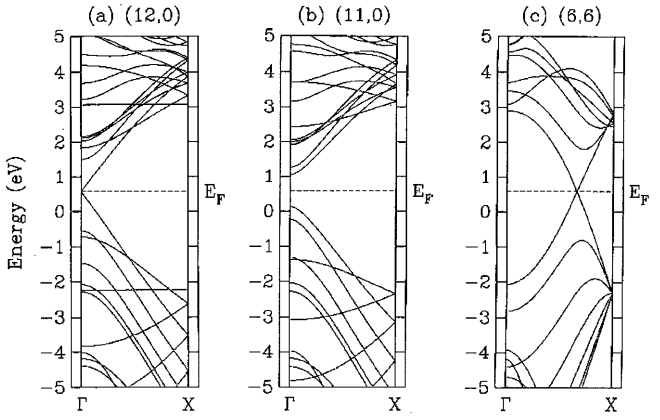

Fig. 2. Band structures of a $(12, 0)$ zigzag tubule (**a**), a $(11, 0)$ zigzag tubule (**b**), and a $(6, 6)$ armchair tubule (**c**). The X point has a wave number near $\frac{\pi}{3a_{\mathrm{C-C}}}$ in the zigzag symmetry, and near $\frac{\pi}{\sqrt{3}a_{\mathrm{C-C}}}$ in the armchair one; where $a_{\mathrm{C-C}}$ is the nearest-neighbor C−C distance (1.42 Å)

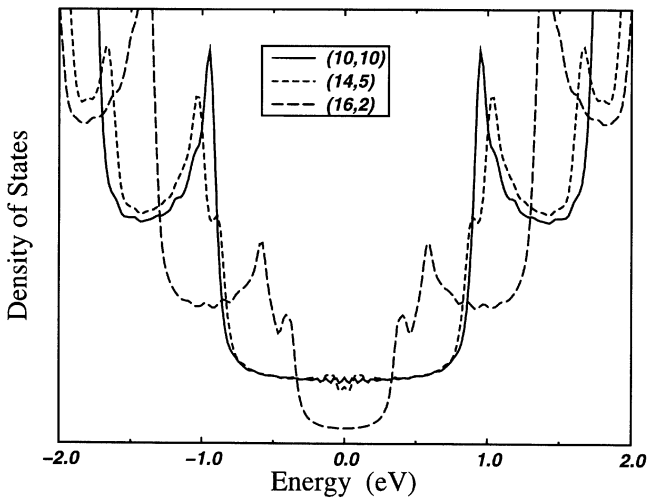

Fig. 3. One-dimensional electronic densities of states of metallic $(14, 5)$ and semiconducting $(16, 2)$ chiral nanotubes, compared to the DOS of metallic $(10, 10)$ achiral nanotube. The Fermi level is positioned at the zero energy. Tight-binding calculations with Slater-Koster hamiltonian are based on the $2p$ valence orbitals of carbon

lower than the Fermi level, while bonding sp^2 σ bands appear at energies lower than -2.5 eV and mix weakly with π bonding states.

The other special class of tubules: the armchair ones, always exhibit a metallic behavior. Figure 2c shows the band structure of an armchair nanotube. The set of wave vectors which are allowed by periodic boundary conditions for an (n, n) armchair tube always contains the K point for all n, because the line crossing the Γ point always crosses the K point. Although the enhancement of the electron transfer along the tubule circumference moves the degenerate point, the latter always remains on the allowed line. Figure 2c presents the band structure of the $(6, 6)$ armchair tubule, showing two bands crossing the Fermi level at the same wave vector, exhibiting a metallic nature.

All other nanotubes are chiral tubes which electronic properties depend on their respective (n, m) characteristic. Figure 3 illustrates the DOS of two chiral nanotubes compared to the DOS of a $(10, 10)$ armchair tube of approximately the same diameter (~ 1.35 nm). The chiral $(14, 5)$ nanotube exhibits a metallic behavior, while the DOS of $(16, 2)$ presents a gap of ~ 0.65 eV. When compared to the $(10, 10)$ tube, the DOS of the metallic chiral tubes does not significantly differ. Our calculations illustrate that van Hove singularities remains sharp and distinctive with a chiral geometry, very much like in the armchair or zigzag wrappings. Although the 1D real space unit cell of a general chiral nanotube is often one order of magnitude larger than the unit cell of an achiral tube (i.e. the unit cell of $(11, 9)$ contains 1204 atoms while it contains only 40 for the $(10, 10)$), the DOS shape does not contain many weak spikes uniformly distributed in energy as previously expected [16]. These results are in complete agreement with the Van Hove singularities (energy threshold for an electronic sub-band caused by the quantum confinement of electrons in the radial and circumferential directions of the nanotube) recently observed [17] in the experimental DOS for both chiral and achiral nanotubes.

In summary, single-wall nanotubes are thus categorized into three classes: the first class consists of metallic tubules (armchair tubes), the second of semiconducting ones with narrow band gaps ($\frac{1}{3}$ of the possible zigzag and chiral tubes), and the third of semiconducting ones with moderate band gaps ($\frac{2}{3}$ of the possible zigzag and chiral tubes). The band gap is tunable by choosing the nanotube structure. It may be surprising that the calculated electronic structure can be either metallic or semiconducting (Fig. 1b) depending on the choice of (n, m), although there is no difference in the local chemical bonding between the carbon atoms in the tubules, and no doping impurities are present.

All the calculated results [10–15] for the 1D electronic structure show that for small diameter single-wall graphene tubes (including chiral ones, Fig. 3), about $\frac{1}{3}$ of the tubules are metallic (or narrow band gap semiconductor), and $\frac{2}{3}$ are semiconducting, depending on the tube diameter D_ϕ and the chiral angle θ. In terms of the integers (n, m), the tube diameter D_ϕ is given by

$$D_\phi = \frac{C_h}{\pi} = \frac{\sqrt{3}a_{\mathrm{C-C}}\sqrt{m^2+mn+n^2}}{\pi}, \tag{1}$$

where $a_{\mathrm{c-c}}$ is the nearest-neighbor C−C distance (1.42 Å), and the chiral angle θ is given by

$$\theta = \tan^{-1}\left[\frac{\sqrt{3}n}{(2m+n)}\right]. \tag{2}$$

Metallic conduction in a single-wall nanotube is achieved when

$$n - m = 3q, \tag{3}$$

where q is an integer. Tubules satisfying (3) are indicated in Fig. 1b as large circles, and these are metallic (or narrow band gap semiconducting) nanotubes. The small circles in the same figure do not satisfy (3) and correspond to wider gap semiconducting tubules.

Metallic 1D energy bands are generally unstable under a Peierls distortion. However, the Peierls energy gap obtained for the metallic tubules is found to be suppressed by increasing the tube diameter, so that the Peierls gap quickly reaches the zero-energy gap of 2D graphite [11, 13]. Thus, if

finite temperatures or fluctuation effects are considered, such a small Peierls gap can be neglected. It is also of interest to note that as the tube diameter increases, more wave vectors are allowed for the circumferential direction, the tubules become more two-dimensional, and the semiconducting band gap disappears [10, 11].

Recently, two teams of experimentalists [17, 18] used scanning tunneling microscope probes at low temperature to test these theoretical predictions, by measuring electronic structure (density of states) and physical structure (the nanotube diameter and helicity), confirming the one-dimensional nature of conduction in single-wall nanotubes.

1.2 Electronic transport

1.2.1 Characteristic lengths, resistance and transmission. The way in which we envisage transport properties depends crucially on the geometric dimensions of the samples with respect to three main characteristic lengths in the conductor. These characteristic lengths with their subtle aspects are of paramount importance in order to understand, even qualitatively, electron propagation in such tiny entities as CNs.

The *elastic mean free path*:

$$L_{\mathrm{el}} = v_{\mathrm{F}} \tau_{\mathrm{el}} \tag{4}$$

which is directly related to the time of flight between two elastic collisions, τ_{el}, is due to collisions with stationary impurities. Through these collisions, electrons exchange momentum but retain their phase memory.

The *phase-coherence length*, is the distance that an electron travels before its initial phase is destroyed:

$$L_\phi = \sqrt{D\tau_\phi} \tag{5}$$

Where D is the diffusion constant. Expression (5) shows that the motion between two phase-randomizing collisions is diffusive.

The *Fermi wavelength*, which is related to the kinetic energy of electrons at the Fermi level:

$$\lambda_{\mathrm{F}} = \frac{2\pi}{k_{\mathrm{F}}} \tag{6}$$

is almost temperature insensitive for metals, but for semiconductors and semimetals, it may vary widely with temperature. Thus for carbons and graphites the two last characteristic lengths are temperature sensitive.

To these three main lengths one should add the *inelastic mean free path*, L_{in} which is the distance that an electron travels between two inelastic collisions, such as electron-phonon or electron-electron collisions. Since, except for some specific situations [19], inelastic collisions destroy the phase coherence, the inelastic mean free path is generally equal to the phase coherence length. Note too that, while there is an exchange of momentum in an electron-phonon collision, in an electron-electron collision, momentum is conserved after collision. Electron-electron collisions are phase-randomizing collisions that do not affect the electron free path.

One should also consider the *thermal length*:

$$L_{\mathrm{T}} = \sqrt{\frac{\hbar D}{kT}} \tag{7}$$

which is of interest when discussing transport in mesoscopic systems (Sect. 2.1), the *magnetic length*:

$$L_\phi = \sqrt{\frac{\hbar}{qB}} \tag{8}$$

and the *cyclotron radius*:

$$L_{\mathrm{c}} = \frac{\hbar k_{\mathrm{F}}}{qB} \tag{9}$$

which should be taken into account in the presence of an applied magnetic field, B.

For macroscopic samples, i.e. samples with dimensions much higher than these characteristic lengths, and at high enough temperatures, we do not have to worry about the phase of the electron waves. Inelastic collisions are dominant, mainly through electron-phonon interactions, where the phase memory of electrons is lost together with their momentum. We are in the situation of diffusive motion described in Sect. 1.2.3 and the regime is ohmic. If the temperature is lowered, the inelastic mean free path increases and, eventually, becomes much larger than the elastic mean free path. Through elastic collisions, electrons loose momentum but not their phase memory. Interferences may show up in the electronic system generating weak localization effects (Sect. 1.2.4), whatever the geometrical dimensions of the sample. Thus, quantum effects are observed in a macroscopic sample, which is the case for bulk carbons and graphites. When, in addition, the sample has dimensions comparable to the main characteristic lengths described above, additional quantum effects may show up in the presence of a magnetic field in the form of Aharonov-Bohm oscillations and universal conductance fluctuations.

At low temperatures, in a metal sample of very small dimensions, though larger than that of the atom, it may happen that the phase-coherence length (5) becomes larger than the dimensions of the sample. In a perfect crystal, the electrons will propagate ballistically from one end of the sample and we enter into a *ballistic regime* where the laws of conductivity discussed below Sect. 1.2.3 no more apply. The propagation of an electron is then directly related to the quantum probability of transmission across the global potential of the sample.

However, static defects will scatter electrons elastically in a real crystal. We are then in a situation where electrons do not loose memory of the phase contained in their wave function and thus propagate through the sample in a coherent way. Electrons in a given state interacting with the same impurity experience the same phase shift and the geometrical configuration of impurities will thus have a direct effect on electron propagation. This happens in *mesoscopic systems* such as CNs (Sect. 2.1.2).

1.2.2 Semimetallic behavior. Pristine HOPG is a semimetal with an equal and relatively small density of electrons and holes, while some carbons are narrow-gap semiconductors [20]. Carbons and graphites have also generally two types of charge carriers in small densities. The semimetallic behavior of graphites, due to their small Fermi surfaces, have a dramatic effect on the band structure and on the scattering mechanisms:

– at low temperatures, the charge carrier system is fully degenerate. When the temperature increases, the carrier distributions become partially degenerate and the parameters of the band structure and Fermi surface, and thus the carrier densities, become very sensitive to temperature,
– owing to these small Fermi surfaces, electron-phonon scattering is particularily weak leading to very high carrier mobilities. We have previously introduced [2] the concept of the *ineffectiveness of phonon scattering* in graphites. This results in unusually high inelastic relaxation times which allows the observation of quantum interferences and mesoscopic regime at much higher temperatures than in metals. Also, weak electron-phonon interaction associated to weak disorder allows the observation of electron-electron scattering, which can hardly be observed in other types of solids.
– weak electron-point defect scattering associated to large Fermi wavelengths. From Raleigh's law it is known that point defect scattering depends dramatically on the scattered wave wavelength. This is the case for electrons.

We have previously discussed the electron-phonon interaction in the particular case of pristine graphite [2, 21]. It was shown that, contrary to 3D metals, the quasi-2D electron and hole systems in semimetallic graphites do not interact with the same class of phonons. This reason leads to the ineffectiveness of phonon scattering. For small Fermi surfaces, like those characterizing semimetals, in order to satisfy energy and momentum conservation requirements, electrons and holes are scattered through large angles by low energy *subthermal phonons*, except at very low temperatures. The limit is determined by a characteristic temperature:

$$\theta^* = \frac{2k_F v_s \hbar}{k_B} \tag{10}$$

The subthermal phonons are of lower frequencies than the thermal phonons which dominate at the temperature considered and are thus less numerous and the resulting electron-phonon scattering is less effective, even for large angle scattering.

For graphite, the velocity of sound in the graphene planes, $v_s \sim 2.1 \times 10^6$ cm/s, is one order of magnitude higher than in metals, while k_F, the Fermi wave vector, is orders of magnitudes smaller than in ordinary metals. The result is that θ^* is much smaller than the Debye temperature of 3D metals and, a *fortiori*, of the in-plane Debye temperature of graphite.

The very high charge carriers mobilities observed in graphites is also due to the very low effective masses in some directions and the low dimensionality of the electronic system.

1.2.3 Semiclassical transport in the diffusive regime. For a given group of charge carriers the Drude electrical conductivity is expressed:

$$\sigma = \frac{q^2 N_\tau}{m^*} \tag{11}$$

where q is the electronic charge, N is the charge carrier density, τ the relaxation time and m^* the carrier effective mass. The mobility which describes diffusive motion is expressed:

$$\mu = \frac{v_d}{E} \tag{12}$$

In a naive way, one may imagine the mobility, which is defined as the drift velocity, v_d, of the charge carriers per unit electric field, E, as expressing the easiness with which the carriers move in the crystal lattice.

Equation (11) for diffusive motion apply for macroscopic systems, i.e. of dimensions larger than the characteristic lengths defined above, whatever their dimensionality.

If there are electrons and positive holes, as in pristine graphites, the contribution of each type of carriers should be taken into account. In that case, the total electrical conductivity (σ) is given by the sum of the partial conductivities, σ_j, of each group of charge carriers, j:

$$\sigma = \sum_j \sigma_j \tag{13}$$

When there is more than one scattering mechanism, s, experienced by electrons and when the relaxation times describing these scattering events, τ_s, are of the same order of magnitude, then the total relaxation time τ is a combination of these τ_s and is given by Matthiessen's rule, which is expressed:

$$\frac{1}{\tau} = \sum_s \frac{1}{\tau_s} \tag{14}$$

provided the various types of scattering may be considered as independent and the associated relaxation time isotropic. These assumptions are only partly true in many systems including graphites.

The main contributions to the classical scattering mechanisms in metals consist in an intrinsic temperature dependent *ideal* relaxation time, which is mainly due to electron-phonon interactions, and an extrinsic *residual* temperature independent term due to static lattice defects.

When a magnetic field is applied to a conductor carrying an electrical current its resistance increases due to the effect of the Lorentz force on the charge carriers. This is the so-called *magnetoresistance* effect. The fractional change in the resistance caused by the application of an external magnetic field is expressed:

$$\frac{\Delta\varrho}{\varrho_0} = \frac{\varrho_H - \varrho_0}{\varrho_0} \tag{15}$$

where ϱ_H and ϱ_0 are the electrical resistivities with and without magnetic field respectively. At low magnetic fields, the magnetoresistance depends essentially on the carrier mobilities.

However, an inverse effect, i.e. a decrease of resistance with increasing magnetic field, *negative magnetoresistances*, have been observed in pregraphitic carbons by Mrozowski et al. [22] as well as in other forms of carbons (Sect. 1.2.4).

1.2.4 Quantum interferences. In the presence of weak disorder, one should consider an additional contribution to the residual resistivity due to *weak localization* resulting from quantum interference effects and/or that due to *Coulomb interaction* effects. These quantum effects, though they do not generally affect significantly the magnitude of the resistivity, introduce new features in the low temperature transport effects. So in addition to the semiclassical ideal and residual

resistivities of carbons discussed above, we must take into account the contributions due to quantum localization and interaction effects. These effects were found to confirm the 2D character of conduction in turbostratic carbons [23] (including MWNTs) and acceptor GICs [24, 25].

In the same way, experiments performed at the mesoscopic scale in CNs revealed quantum oscillations in the electrical conductance as a function of magnetic field, the so-called universal conductance fluctuations (UCF).

The quantum interference phenomenon leads to an increased backscattering probability with respect to the semiclassical value and thus to a larger resistivity. This effect which tends to localize electrons through increasing backscattering is called *weak localization*. It gives rise to characteristic resistivity variations with temperature and magnetic field.

When the temperature decreases, the inelastic lifetime τ_{in} due to electron-phonon or electron-electron interactions increases. As a result, the number of sequences leading to constructive inteferences increases and backscattering is more efficient. This results in an increased resistivity as the temperature is decreased. When the temperature increases, the inverse situation occurs and when electron-phonon or electron-electron interactions are so numerous that the inelastic lifetime, τ_{in}, is of the order of τ_{el}, the electron looses its phase memory after each collision and we are back in the semiclassical situation.

It was demonstrated that when a *magnetic field* is applied to a sample it decreases the effect of the constructive interferences. This effect is more pronounced for longer sequences. The magnetic field reduces the backscattering probability tending to restore the semiclassical resistivity and thus leads to a decrease of the measured resistivity. One speaks about *negative magnetoresistance*. This effect has nothing to do with the conventional *positive magnetoresistance* which is generally observed in electrical conductors and was defined above Sect. 1.2.3. In the case of positive magnetoresistance, the Lorentz force due to the magnetic field deviates electrons from their initial path and increases the resistivity in the applied electric field direction.

The limit of weak disorder, which is also the condition for the Boltzmann approximation to hold, implies that the electron mean free path, L, should be large compared to its wavelength, i.e.:

$$k_F L \gg 1 \tag{16}$$

where k_F is the Fermi wave number. When these two terms are of the same magnitude, we are in a situation of strong disorder and strong localization.

In a 2D system, when this last condition is fulfilled, and when $\tau_{el} \ll \tau_{in}$, the correction to the classical conductivity is:

$$\delta\sigma_{2D} = -\frac{q^2}{2\pi^2\hbar} \ln\left\{\frac{\tau_{in}}{\tau_{el}}\right\} \tag{17}$$

and if:

$$\tau_{in} = aT^{-p} \tag{18}$$

we get:

$$\delta\sigma_{2D} = -\frac{p}{2}\frac{q^2}{\pi^2\hbar} \ln\left\{\frac{T}{T_0}\right\} \tag{19}$$

The requirement that $\tau_{el} \ll \tau_{in}$ allows the electrons to experience many elastic collisions leading to constructive interferences before they are inelastically scattered and loose their phase memory.

2 Experimental findings

2.1 Multi-wall nanotubes

2.1.1 Diffusive transport. At high temperature, MWNTs behave much like bulk graphite [26] and can be described, in the thermodynamic limit, by means of semiclassical models describing diffusive motion Sect. 1.2.3. At low temperature, weak localization effects are observed as for the case of bulk graphites, but in addition when the temperature and sizes are low enough to realize mesoscopic conditions, specific quantum effects are observed (UCFs).

The electrical resistivity of carbon-based materials decreases with increasing structural perfection. Generally, the differences observed between samples are more pronounced when the heat treatment temperature (HTT) varies within one class of carbon-based materials than they are between various classes for samples heat treated at approximately the same HTT.

Samples of *high structural perfection* exhibit resistivities lower than a few $10^{-6}\,\Omega$m. In that case observed resistivities may be described using the semimetallic graphite band model. Around room temperature, the charge carriers are scattered by defects and phonons. Contrary to metals, where the highly degenerate electron system is temperature insensitive and only the mobility varies with temperature, in a semimetal like graphite, because of the very small carrier densities, these are also very sensitive to defects and temperature. This is exactly the situation in MWNT.

In Fig. 4, we report on measurements of the temperature dependence of the zero-field electrical resistivitivity [27]. It may be seen that, above 2 K, the temperature dependence of the zero-field resistivity of MWNTs is governed by the temperature dependence of the carrier densities and may be described by the simple two-band (STB) model derived by Klein [28] for electrons, n, and holes, p, densities in semimetallic graphite:

$$n = C_n k_B T \ln\left\{1 + \exp\left\{\frac{\varepsilon_F}{k_B}\right\}\right\} \tag{20}$$

and

$$p = C_p k_B T \ln\left\{1 + \exp\left\{\frac{\Delta - \varepsilon_F}{k_B T}\right\}\right\} \tag{21}$$

where ε_F is the Fermi energy and Δ is the band overlap. C_n and C_p are the fitting parameters.

A value of $\Delta \sim 4$ meV is obtained for the band overlap, with the Fermi energy right in the middle of the overlap. This value of the overlap has to be compared to that of 40 meV for crystalline graphite. The difference was ascribed to the turbostratic stacking of the adjacent layers which should reduce drastically the interlayer interactions, like in disordered graphite. The smaller overlap implies also that, within the frame of the STB model, the carrier density is 10 times smaller than in graphite.

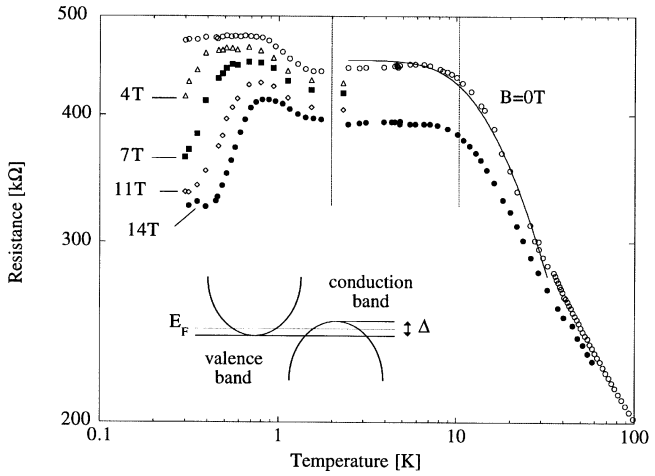

Fig. 4. Electrical resistance as a function of the temperature at the indicated magnetic fields for a bundle of nanotubes. The *dashed lines* separate three temperature ranges (see text), while the continuous curve is a fit using the two-band model for graphite (see inset) with an overlap of 3.7 meV and a Fermi level right in the middle of the overlap [26]

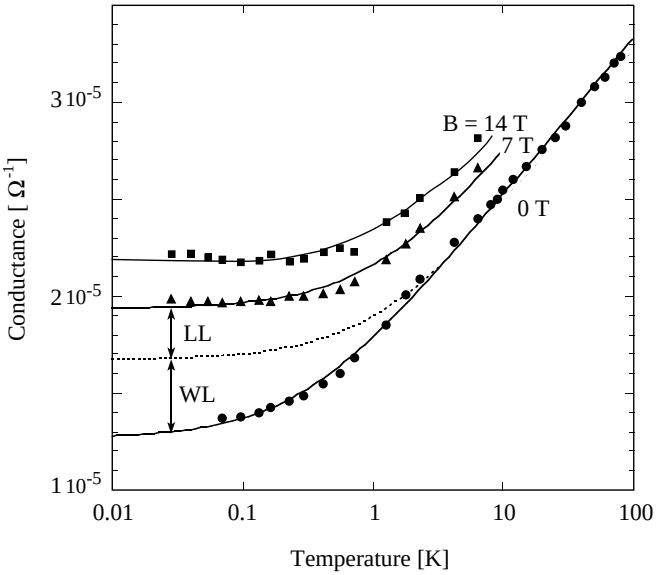

Fig. 5. Electrical conductance as a function of temperature at the indicated magnetic fields. The *solid line* are fits by $G(T) = G(0) + \frac{e^2}{2\pi_2\hbar}\frac{n\pi d}{L}\ln\left[1+\left(\frac{T}{T_c(B,\tau_S)}\right)^p\right]$ with parameters $p = 1$, $n = 4$, and $T_c = 0.3$, 1.1, and 1.5 K at $B = 0$, 7, and 14 T, respectively. The *dashed line* separates the contributions to the magnetoconductance of the Landau levels and the weak localization

2.1.2 2D localization and universal conductance fluctuations. The particular geometry and the varying defect structure of carbon fibers have allowed the observation of quantum transport effects in these materials. These were first observed by Piraux et al. [24] in intercalated acceptor carbon fibers, then on pristine fibers [23] and more recently on nanotubes [27]. The observed negative magnetoresistance in pristine carbon fibers, which is one of the signatures of the two-dimensional (2D) weak localization, was attributed to the turbostratic layers.

Weak localization effects were also observed on individual multi-wall carbon nanotubes (MWNT) [27]. In Fig. 5 we present the temperature dependence of the conductance for one of the carbon nanotubes measured respectively in a magnetic field of 7 T and 14 T. The measured multi-wall carbon nanotube had a diameter of about 20 nm and a total length of the order of 1 μm. In zero magnetic field, a logarithmic decrease of the conductance at higher temperature, followed by a saturation of the conductance at very low temperature, was observed. The saturation occurs at a critical temperature, $T_c = 0.3$ K at zero magnetic field, which shifts to higher temperatures in the presence of a magnetic field. The data in Fig. 5 show also that there is an additional contribution to the magnetoconductance of the carbon nanotube which is temperature independent up to the highest temperature investigated, including in the logarithmic temperature variation range. This magnetoconductance was ascribed to the formation of Landau states predicted by Ajiki et al. [29]. Both 2D weak localization and "Landau level" contributions to the magnetoconductance can be separated as illustrated in Fig. 5.

The temperature and field dependences of the nanotube conductance were interpreted consistently in the frame of the theory for 2D weak localization that we previously discussed (Sect. 1.2.4). Owing to the very small dimensions of the sample, the samples were found to be close to the mesoscopic regime in the lowest temperature range.

As may be seen from Fig. 6, reproducible aperiodic fluctuations appear in the magnetoconductance with temperature independent peaks and valleys positions with respect to magnetic field. In Fig. 7, we present the temperature dependence of the peak-to-peak amplitude of the conductance fluctuations for three selected peaks as well as the rms amplitude of the fluctuations, rms[δG]. The amplitude of the fluctuations are constant in the lower temperature range, then decreases slowly with increasing temperature following a weak power law. The turnover in the temperature dependence of the conductance fluctuations occurs at a critical temperature $T_c^* \approx 0.3$ K, which, in contrast to the T_c values characteristic of weak localization effects, is independent of the magnetic field (Fig. 7). This behavior was interpreted in terms of *universal conductance fluctuations* (UCF) previously observed in mesoscopic weakly disordered metals and semiconductors. In such systems, where the size of the sample, L, is smaller or comparable to both L_ϕ, the phase-coherence length, and the thermal diffusion length L_T, elastic scattering of electron wave functions generate an interference pattern which gives rise to a sample-specific, time-independent correction to the classical conductance. An applied magnetic field, by tuning the phase of the electrons, can modify the interference pattern, and hence the correction to the conductance. The universal character of the phenomenon (UCFs) stems from the fact that the amplitude of the fluctuations δG has a universal value: rms[δG]$\approx q^2/h$ as long as the sample size L is smaller than L_ϕ and L_T. When the relevant length scale, L_ϕ or L_T, becomes smaller than L, the amplitude of the observed fluctuations decreases due to self-averaging of the UCF in phase-coherent subunits. The amplitude of the universal conductance fluctuations (for mesoscopic 2D systems) decreases as a weak power law $T^{-\alpha}$ where α depends on dimensionality and limiting diffusion length, L_ϕ or L_T ($\alpha = 1/2$ for a 2D system with $L_\phi < L, L_T$).

So, in spite of the small diameter of the MWNT compared to the Fermi wavelengths of the charge carriers, the cylindrical structure of the honeycomb lattice gives rise to a 2D electron system for both weak localization and universal con-

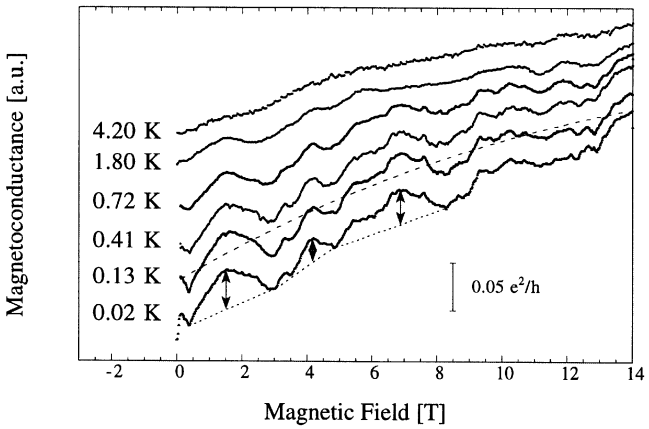

Fig. 6. Magnetic field dependence of the magnetoconductance at different temperatures [27]

ductance fluctuation effects. Both the amplitude and the temperature dependence of the conductance fluctuations are consistent with the universal conductance fluctuations models applied to the particular cylindrical structure of nanotubes [27]. At high temperature a behavior similar to that known for bulk graphites was observed. This is in contrast to what was very recently observed on single-wall nanotubes.

2.2 Single-wall nanotubes

Although experiments on individual multi-wall nanotubes did detect a variety of novel electrical properties, including 2D quantum interference effects due to weak localization and universal-conductance fluctuations, they did not illustrate any one-dimensional quantum effects, essentially because the diameters of the nanotubes were too large (or the temperature too high to detect them). In addition, the experimental results from MWNTs are difficult to analyze due to simultaneous contributions of concentric nanotubes with different diameters and chiralities.

Experiments performed in Delft on individual single-wall nanotubes [30] have confirmed their one- dimensional nature. They appear to behave as a genuine coherent quantum wires,

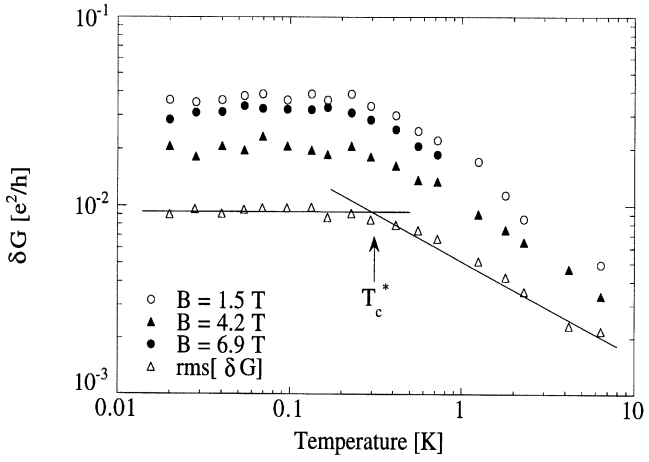

Fig. 7. Temperature dependence of the amplitude of δG for three selected peaks (see arrows in Fig. 6) as weil as rms[δG] [27]

or quantum dots if the length of the tube is reduced. Although nanotubes are very much longer than they are wide, the finite length of then tubes still limits the number of allowed wavectors along the nanotube axis. This gives rise to discrete energy states, which can be determined by measuring the conductance as a function of the voltage. For a nanotube 3 μm long, the Delft group [30] found that discrete states near the Fermi level are separated by about 0.4 meV. This value is consistent with a "particle-in-a-box" energy separation between levels of a 3-μm-long 1D tube:

$$\Delta E = \frac{h v_{\mathrm{F}}}{2L} \sim 0.6\,\mathrm{meV} \tag{22}$$

where the Fermi velocity is estimated to $v_{\mathrm{F}} \sim 8.1 \times 10^5\,\mathrm{ms}^{-1}$, and L is the nanotube length.

Coulomb charging effects have also been observed in this 1D system. The energy needed to add an electron to a single-wall nanotube is 2.6 meV, energy needed to overcome the Coulomb repulsion between electrons. Coulomb charging occurs when the contact resistance is larger than the quantum resistance ($R_K = \frac{h}{e} \sim 26\,\mathrm{k\Omega}$) and when the total capacitance C of the object is so small that adding a single electron costs a significant charging energy:

$$E_c = \frac{e^2}{C} \sim 2.5\,\mathrm{meV} \tag{23}$$

where $C \sim 3 \times 10^{17}\,\mathrm{F}$ is estimated as the geometrical self-capacitance of a 3-μm-long tube. At low temperature, that is $k_{\mathrm{B}}T \ll E_{\mathrm{c}}$, the current is thus blocked (Coulomb Blockade) and will flow only when a threshold bias voltage will be applied ($V_{\mathrm{bias}} > \frac{e}{2C}$).

The electrical properties of individual bundles (ropes) of single-wall nanotubes have also been measured [31]. Peaks were also observed in the conductance as a function of the gate voltage that modulated the number of electrons in the rope. These results were interpreted in terms of single-electron charging and resonant tunneling through the quantized energy levels of the 1D single-wall nanotube composing the rope. Although the close-packing of individual SWNTs into ropes does not change significantly their electronic properties, recent calculations [32] show that the interaction between tubes in a rope could induce a pseudogap of about 0.1 eV at the Fermi level. This pseudogap strongly modifies many of the fundamental electronic properties, thus predicting a semimetal-like temperature dependence of the electrical conductivity. The existence of both electron and hole charge carriers would lead to qualitatively different thermopower and Hall-effect behaviors from those expected from a normal metal.

Since nanotubes are typically a few microns long, electrical contacts can be made by modern lithography techniques. Single-wall carbon nanotubes thus provide a unique system for studying single-molecule transistor effects, in which an electrode (V_{gate}) close to the conducting nanotube is used to modulate the conductance [33].

Unfortunately, the group of Delft could not establish the structural (n, m) parameters of the samples, so a direct link to a theoretical simulation was not possible. The next step will be to achieve this link, so that quantum transport measurements (current-voltage characteristics) from a perfectly characterized (n and m are known) single-wall nanotube can be compared to a theoretical calculation.

3 Conclusion

In the present paper, we show that the low temperature electrical transport in a multi-wall carbon nanotube is governed by typical electron interference effects occuring in disordered conductors of reduced dimensionality. Despite their very small diameter, the cylindrical structure of the honeycomb gives rise to a two-dimensional electrical conduction process. The temperature and magnetic field dependences of both the weak localization effects and the universal conductance fluctuations can be explained consistently in terms of existing theoretical models, provided the typical cylindrical geometry of the carbon nanotube is taken into account.

On the other hand, due to the structural symmetry of the single-wall nanotubes, the electronic wavefunction may extend over the entire tube, thus confirming their one-dimensional nature. Recent electrical transport measurements [30] on individual SWNTs show that conduction seems to occur through well separated, discrete electron states that are quantum-mechanically coherent over long distances.

Multi-wall and single-wall carbon nanotubes are found to be interesting systems where different quantum aspects of conduction are observed, mostly due to their low dimensionalities and small dimensions. In order to tailor their electronic properties, and consequently the type and range of conductivities, doping and/or intercalation will certainly lead to intense research in the next few years.

Acknowledgements. JCC acknowledges the National Fund for Scientific Research [FNRS] of Belgium for financial support. This paper presents research results of the Belgian Program on Interuniversity Attraction Poles on Reduced Dimensionality Systems (PAI-IUAP N. P4/10) initiated by the Belgian Federal OSTC.

References

1. J.-C. Charlier, J.-P. Issi: Physics and Chemistry of Solids **57**, 957 (1996)
2. J.-P. Issi: In *World of Carbon*, ed. by P. Delhaes (Gordon and Breach, UK 1998)
3. J.-C. Charlier, X. Gonze, and J.-P. Michenaud: Carbon **32**, 289 (1994)
4. M.S. Dresselhaus, G. Dresselhaus, P.C. Eklund: *Science of Fallerenes and Carbon Nanotubes* (Academic Press, San Diego 1996)
5. S. Iijima, T. Ichihashi: Nature **363**, 603 (1993)
6. D.S. Bethune, C.H. Klang, M.S. de Vries, G. Gorman, R. Savoy, J. Vazquez, R. Beyers: Nature **363**, 605 (1993)
7. S. Iijima: Nature **354**, 56 (1991)
8. T.W. Ebbesen, H. Hiura, J. Fujita, Y. Ochiai, S. Matsui, K. Tanigaki: Chem. Phys. Lett. **209**, 83 (1993)
9. A. Thess, R. Lee, P. Nikolaev, H. Dai, P. Petit, J. Robert, C. Xu, Y.H. Lee, S.G. Kim, D.T. Colbert, G. Scuseria, D. Tomanek, J.E. Fischer, R.E. Smalley: Science **273**, 483 (1996)
10. N. Hamada, S. Sawada, A. Oshiyama: Phys. Rev. Lett. **68**, 1579 (1992)
11. R. Saito, M. Fujita, G. Dresselhaus, M.S. Dresselhaus: Appl. Phys. Lett. **60**, 2204 (1992); *ibidem*: Phys. Rev. B **46**, 1804 (1992)
12. K. Tanaka, K. Okahara, M. Okada, T. Yamabe: Chem. Phys. Lett. **191**, 469 (1992)
13. J.W. Mintmire, B.I. Dunlap, C.T. White: Phys. Rev. Lett. **68**, 631 (1992)
14. K. Harigaya: Phys. Rev. B **45**, 12071 (1992)
15. C.T. White, D.H. Robertson, J.W. Mintmire: Phys. Rev. B **47**, 5485 (1993)
16. M.S. Dresselhaus: Nature **391**, 19-20 (1998)
17. J.W.G. Wildöer, L.C. Venema, A.G. Rinzler, R.E. Smalley, C. Dekker: Nature **391**, 59 (1998)
18. T.W. Odom, J.-L. Huang, P. Kim, C.M. Lieber: Nature **391**, 62 (1998)
19. S. Datta: *Electronic Transport in Mesoscopic Systems* (Cambridge University Press 1995)
20. M.S. Dresselhaus, G. Dresselhaus, R. Saito: Electronic Band Structure of Graphites In *World of Carbon*, ed. by P. Delhaes (Gordon and Breach, UK 1998)
21. J.-P. Issi, B. Nysten: Electrical and thermal transport properties in carbon fibers In *Carbon Fibers*, ed. by J-B. Donet (in press 1998)
22. S. Mrozowski, A. Chaberski: Phys. Rev. **104**, 74 (1956)
23. V. Bayot, L. Piraux, J.-P. Michenaud, J.-P. Issi: Phys. Rev. B **40**, 3514 (1989)
24. L. Piraux, J.-P. Issi, J.-P. Michenaud, E. McRae, J.-F. Mareche: Solid State. Commun. **567**, 6 (1985)
25. L. Piraux, V. Bayot, X. Gonze, J.-P. Michenaud, J.-P. Issi: Phys. Rev. B **36**, 9045 (1987)
26. L. Langer, L. Stockman, J.P. Heremans, V. Bayot, C.H. Olk, C. Van Haesendonck, Y. Brnynseraede, J.-P. Issi: J. Mat. Res. **9**, 927 (1994)
27. L. Langer, V. Bayot, E. Grivei, J.-P. Issi, J.P. Heremans, C.H. Olk, L. Stockman, C. Van Haesendonck, Y. Bruynseraede: Phys. Rev. Lett. **76**, 479 (1996)
28. C.A. Klein: J. Appl. Phys. **35**, 2947 (1964)
29. H. Ajiki, T. Ando: J. Phys. Soc. Jpn. **62**, 1255 (1993)
30. S.J. Tans, M.H. Devoret, H. Dai, A. Thess, R.E. Smaller, L.J. Geerligs, C. Dekker: Nature **386**, 474 (1997)
31. M. Bockrath, D.H. Cobden, P.L. McEuen, N.G. Chopra, A. Zettl, A. Thess, R.E. Smalley: Science **275**, 1922 (1997)
32. P. Delaney, H.J. Choi, J. Ihm, S.G. Louie, M.L. Cohen: Nature **391**, 466 (1998)
33. M.S. Dresselhaus, G. Dresselhaus, P. Eklund, R. Saito: Phys. World **33**, January 1998